O. Barry[1]
College of Engineering and Technology,
Central Michigan University,
Mount Pleasant, MI 48859
e-mail: barry1o@cmich.edu

R. Long
College of Engineering and Technology,
Central Michigan University,
Mount Pleasant, MI 48859

D. C. D. Oguamanam
Department of Mechanical and
Industrial Engineering,
Ryerson University,
Toronto, ON M5B 2K3, Canada

Rational Damping Arrangement Design for Transmission Lines Vibrations: Analytical and Experimental Analysis

The control of overhead transmission lines vibrations is achieved by Stockbridge dampers. However, the effectiveness of the damper is significantly dependent on its location on the conductor. This paper studies the arrangement of Stockbridge dampers on power lines vibrations using both analytical and experimental approaches. An explicit expression of the loop length is presented for the first time. This expression is used to determine the optimal damper location based on a rational approach. The effectiveness of the proposed approach is validated numerically and experimentally. The results show very good agreement and indicate that Stockbridge dampers are more effective for asymmetrical damping arrangement with the bigger counterweight oriented toward the tower.
[DOI: 10.1115/1.4035455]

Keywords: Stockbridge damper, optimization, Strouhal frequency, messenger

1 Introduction

The control of the vibrations of overhead transmission lines has been a subject of study for decades. The wind speeds associated with the vibrations vary from 1 to 7 m/s [1]. Stockbridge damper is one of the most common devices used to reduce these vibrations. The effectiveness of the Stockbridge damper is dependent on the damper parameters and its arrangement on the transmission lines [2–5]. While analytical models of the vibrations of transmission lines abound in the literature, see, for example, Refs. [6–11], these studies have ignored the role of the arrangement of Stockbridge dampers. The few studies that examine Stockbridge damping arrangement include Refs. [1] and [3].

The state-of-the art on damper placement is based on a rule of thumb: place the damper symmetrically between 70% and 80% of the loop length corresponding to the highest wind speed (7 m/s) [1]. This recommendation is pragmatic as it facilitates the easy installation of the dampers by construction workers because the damper location usually falls within a few meters from the suspension clamps.

It is expected that the maximum vibration for odd modes occurs at midspan. Hence, it may be reasonable to place a damper at midspan. However, field investigations have shown that a damper located at midspan or further from the suspension clamp has increased probability to experience premature or early fatigue failure due to galloping.

The object of this work reported herein is to revisit the above-mentioned recommendation for determining the optimal damper location as provided in Ref. [1] by expanding the range of wind speed considered to include both medium (4 m/s) and low wind speed (2 m/s), as opposed to employing only the high wind speed. This is achieved by investigating the minimum value of the conductor response as the damper location varies throughout the loop length corresponding to wind speeds of 2, 4, and 7 m/s. The accuracy of the proposed approach is verified experimentally by using the results obtained from the experiment and numerically by using the optimization MATLAB built-in function *fmincon*.

[1]Corresponding author.

Contributed by the Dynamic Systems Division of ASME for publication in the Journal of Dynamic Systems, Measurement, and Control. Manuscript received November 18, 2015; final manuscript received December 1, 2016; published online March 22, 2017. Assoc. Editor: Dumitru I. Caruntu.

2 Analytical Formulation

A schematic of the conductor with a Stockbridge damper is depicted in Fig. 1 and following Ref. [9], the governing equation of motion can be expressed as

$$\{\ddot{q}_r\} + [\omega_r]^2\{q_r\} + 2\zeta[\omega_r]\{\dot{q}_r\} = [F_r] \tag{1}$$

where

$$[\omega_r]^2 = [K_{\mathrm{rr}}][M_{\mathrm{rr}}]^{-1} \tag{2}$$

$$\begin{aligned} M_{\mathrm{rr}} = \sum_{i=1}^{2}\Bigg\{ & m_{\mathrm{c}}\int_0^{L_{\mathrm{ci}}} {Y_{\mathrm{ci}}^{(r)}}^2 dx + m_{\mathrm{m}}\int_0^{L_{\mathrm{mi}}} {Y_{\mathrm{mi}}^{(r)}}^2 dx_{\mathrm{m}} + {Y_{\mathrm{c1}}^{(r)}}^{2*}(m_{\mathrm{i}} + m_{\mathrm{m}}L_{\mathrm{mi}}) \\ & + {Y_{\mathrm{c1}}^{(r)}}^{2*\prime}\left[m_{\mathrm{i}}\left(L_{\mathrm{mi}}^2 + h^2\right) + I_{\mathrm{i}} + h^2 m_{\mathrm{m}}L_{\mathrm{mi}} + \frac{1}{3}L_{\mathrm{mi}}^3\right] \\ & + {Y_{\mathrm{mi}}^{(r)}}^{2*} m_{\mathrm{mi}} + {Y_{\mathrm{mi}}^{(r)}}^{2*\prime} I_{\mathrm{i}} + (-1)^{(\mathrm{i}+1)}2m_{\mathrm{i}}L_{\mathrm{mi}}{Y_{\mathrm{c1}}^{(r)}}^{*\prime}{Y_{\mathrm{c1}}^{(r)}}^{*} \\ & + 2m_{\mathrm{mi}}{Y_{\mathrm{c1}}^{(r)}}^{*}{Y_{\mathrm{mi}}^{(r)}}^{*} + 2m_{\mathrm{m}}\int_0^{L_{\mathrm{mi}}} {Y_{\mathrm{c1}}^{(r)}}^{*} Y_{\mathrm{mi}}^{(r)} dx_{\mathrm{m}} \\ & + (-1)^{(\mathrm{i}+1)} m_{\mathrm{m}}L_{\mathrm{mi}}^2 {Y_{\mathrm{c1}}^{(r)}}^{*}{Y_{\mathrm{c1}}^{(r)}}^{*\prime} + (-1)^{(\mathrm{i}+1)}2m_{\mathrm{i}}L_{\mathrm{mi}}{Y_{\mathrm{c1}}^{(r)}}^{*\prime}{Y_{\mathrm{mi}}^{(r)}}^{*} \\ & + (-1)^{(\mathrm{i}+1)}2I_{\mathrm{i}}{Y_{\mathrm{c1}}^{(r)}}^{*\prime}{Y_{\mathrm{mi}}^{(r)}}^{*\prime} + (-1)^{(\mathrm{i}+1)}2m_{\mathrm{m}}\int_0^{L_{\mathrm{mi}}} {Y_{\mathrm{c1}}^{(r)}}^{*\prime} Y_{\mathrm{mi}}^{(r)} dx_{\mathrm{m}} \Bigg\} \end{aligned} \tag{3}$$

$$K_{\mathrm{rr}} = \sum_{i=1}^{2}\left\{\int_0^{L_{\mathrm{ci}}}\left[E_{\mathrm{c}}I_{\mathrm{c}}{Y_{\mathrm{ci}}^{(r)}}^{2\prime\prime} - T{Y_{\mathrm{ci}}^{(r)}}^{2\prime}\right]dx + E_{\mathrm{m}}I_{\mathrm{m}}\int_0^{L_{\mathrm{mi}}} {Y_{\mathrm{mi}}^{(r)}}^{2\prime\prime} dx\right\} \tag{4}$$

$$F_r = F(t)Y_{\mathrm{ci}}\left(x = \frac{L_{\mathrm{c}}}{2}\right) \tag{5}$$

The excitation force is expressed as

$$F(t) = F_0 \sin(2\pi f t) \tag{6}$$

where the expressions of the mode shapes Y_{ci} and Y_{mi} are given in the Appendix. F_0 denotes the excitation force amplitude (N), and f

is the forcing frequency (Hz). m_1 (m_2) is the tip mass on the right-hand (left-hand) side, I_1 (I_2) is the tip rotational inertia on the right-hand (left-hand) side, L_{m_1} (L_{m_2}) is the length of the messenger on the right-hand (left-hand) side, m_c (m_m) is the mass per unit length of the conductor (messenger), m_{m1} (m_{m2}) is the mass of the messenger on the right-hand (left-hand) side, T denotes the conductor tension, E_cI_c (E_mI_m) is the flexural rigidity of the conductor (messenger), (ζ) is the conductor damping ratio, L_c is the conductor span length, Y_{ci} (Y_{mi}) are the mode shapes of the conductor (messenger), and their expressions are given in Ref. [9]. The overdots and primes denote temporal and spatial derivations, respectively.

The expression of the loop length is obtained by equating the natural frequency of the bare conductor to that of the Strouhal frequency (excitation frequency) and solving for L_c/n. The natural frequency of the bare conductor, f_n, is given as [5]

$$f_n = \frac{n}{2L_c}\sqrt{\frac{T}{m_c} + \left(\frac{n\pi}{L_c}\right)^2 \frac{E_cI_c}{m_c}} \tag{7}$$

where n is the mode number. The excitation frequency, f_s, is given as

$$f_s = 0.2\frac{v}{D} \tag{8}$$

where the diameter of the conductor is denoted by D and v represents the wind speed.

At resonance, the natural frequency of the bare conductor is equal to the excitation frequency, thus f_n in Eq. (7) is replaced with f_s, and the resulting expression can be rewritten while denoting the loop length L_c/n as λ such that

$$\lambda = \frac{1}{2f_s}\sqrt{\frac{T}{m_c} + \left(\frac{\pi}{\lambda}\right)^2 \frac{E_cI_c}{m_c}} \tag{9}$$

Squaring both sides of Eq. (9) yields the following expression after some algebraic manipulation:

$$\lambda^4 - \frac{T}{4m_cf_s^2}\lambda^2 - \pi^2\frac{E_cI_c}{4m_cf_s^2} = 0 \tag{10}$$

The loop length is now given as

$$\lambda = \sqrt{\frac{1}{2}\left(\frac{T}{4m_cf_s^2} + \sqrt{\left(\frac{T}{4m_cf_s^2}\right)^2 + \pi^2\frac{E_cI_c}{f_s^2}}\right)} \tag{11}$$

The MATLAB built-in command *fmincon* is used to examine the validity of the proposed algorithm. The approach using *fmincon* involves the determination of the location of the damper that corresponds to the minimum vibration displacement throughout the entire range of excitation frequencies. This optimization problem is posed as

$$\text{Minimize}\left(w_{ci} = \sum_{r=1}^{\infty} q_r(t)Y_{ci}^{(r)}(x)\right) \tag{12}$$

subject to the following constraints:

$$0 \le L_{c1} \le \lambda_{low}$$
$$0 \le L_{c2} \le (L_c - \lambda_{low}) \tag{13}$$

where λ_{low} is the loop length corresponding to low wind speeds. The wavelength being inversely proportional to the frequency (Eq. (11)), λ_{low} is the largest among the three and it can vary in

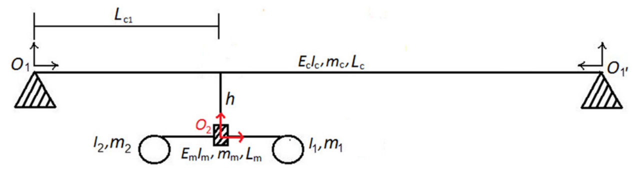

Fig. 1 Schematic of a single conductor with a Stockbridge damper

general between 5 and 10 m depending on the conductor type and wind velocity. This range is considered reasonable for ease installation of dampers. Furthermore, placing the damper too far from the tower will cause the damper to break faster when the conductor is subjected to galloping (high-amplitude low-frequency vibration). This also justifies the reason that the Stockbridge dampers are never placed closer to midspan.

The power equation used for conducting the experiment can be expressed as

$$P_d = FV\cos\theta \tag{14}$$

where P_d is the power dissipated (W), F is the force imparted to the test span at the shaker (N), V is the velocity at the shaker (m/s), and θ is the phase angle between force and velocity (deg).

3 Experiments

A schematic of the test setup is depicted in Fig. 2. The conductor (DRAKE 795 kcmil) was suspended between two steel-reinforced concrete towers as shown in Figs. 3 and 4. The conductor was then tensioned using a cantilever weight arm at one end, and a hydraulic cylinder (Fig. 5) at the other end. A strain gauge load cell (1020 AF-50 kN-B) was placed between the hydraulic cylinder and the dead-end to maintain a desired conductor tension of 20 % rated tensile strength ($T = 28.024$ kN). An electromagnetic shaker, shown in Fig. 6, was installed in the middle of a span length of 27.25 m to excite the conductor at a specific power level. The power level of the system was determined using Eq. (14). One load cell (Dytran106V1) was used along with an accelerometer (B&K 4382) to measure, respectively, the input force from the shaker and the midspan displacement of the conductor. Another accelerometer (B&K 4384) shown in Fig. 7 was placed at an antinode of the corresponding forcing frequency to measure the maximum vibration displacement.

The conductor without dampers was then vibrated at various frequencies. The voltage signal from the load cell and accelerometer was sent through charger amplifiers (Dytran415 and B&K 2635) by means of coaxial cable and then to a digital data-acquisition system (PCI-6034 E) for recording. The key measured data for each frequency consist of a force from the shaker, midspan vibration displacement, free loop vibration amplitude, and phase angle. This procedure was then repeated for a conductor with attached Stockbridge dampers as shown in Fig. 8. Some of the experimental results are summarized in Fig. 9. It is clear from this figure that the attachment of two Stockbridge dampers on the conductor significantly reduces the vibration level of the conductor.

4 Numerical Simulation

The numerical simulations are based on the material properties and parameters in Ref. [9]. The flexural rigidity is $E_cI_c = 1602$ N·m^2, and the linear mass density is $m_c = 1.628$ kg/m.

In the first part of the simulation, the span length is taken to be the same as that used in the experiment ($L_c = 27.25$ m) and only one damper is attached on the cable. The tension is taken to be 28.024 kN, and the applied force is $F_0 = 20$ N. The calculated loop length corresponding to the lowest, medium, and highest wind speed is determined to be 4.6, 2.3, and 1.32 m, respectively. The

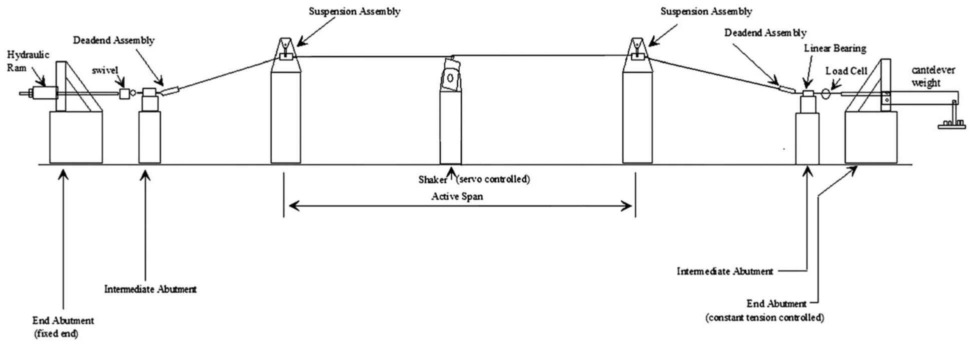

Fig. 2 Schematic of the experimental setup

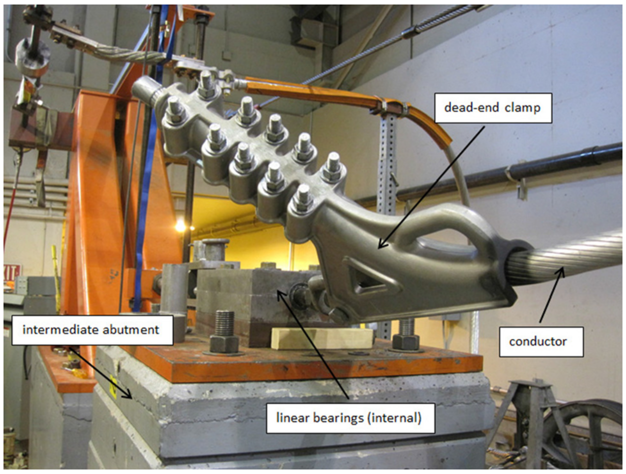

Fig. 3 Abutment

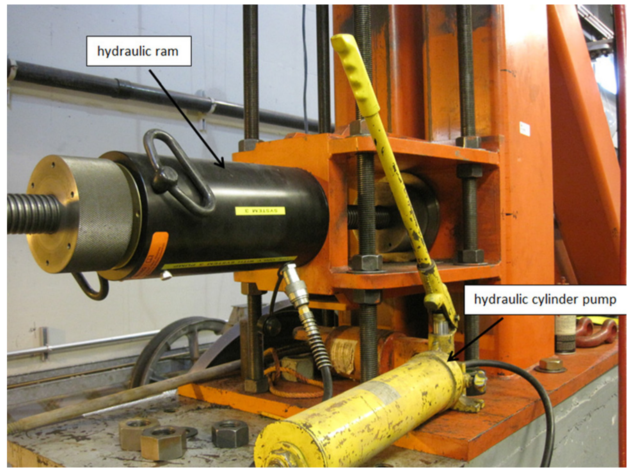

Fig. 5 Hydraulic ram and cylinder

Fig. 4 Steel-reinforced concrete tower

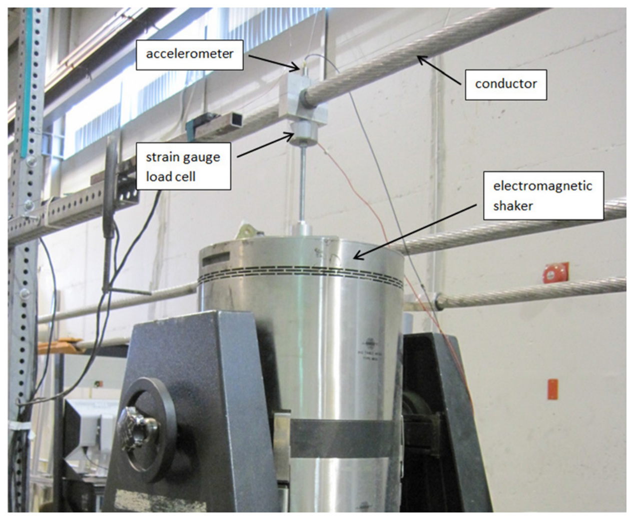

Fig. 6 Electromagnetic shaker

optimization of the damper location corresponding to the low wind speed is depicted in Fig. 10. The results indicate that the optimal damper location for lower frequencies should fall between 50% and 70% of the loop length corresponding to a wind speed of 2 m/s.

In Fig. 11, the optimization is based on medium excitation frequencies. The results show that the vibration amplitude of the conductor is minimum when the damper is positioned between 80% and 90% of the loop length corresponding to a wind speed of 4 m/s. Figure 12 shows the optimization of the damper location based on high frequencies. The results indicate that the optimal location is between 85% and 95%, corresponding to a wind speed of 7 m/s.

The orientation of the damper counterweights is examined to determine the difference of the damper performance when the bigger mass is orientated toward the tower (span-end) and when it is orientated toward the span center. The results are shown in

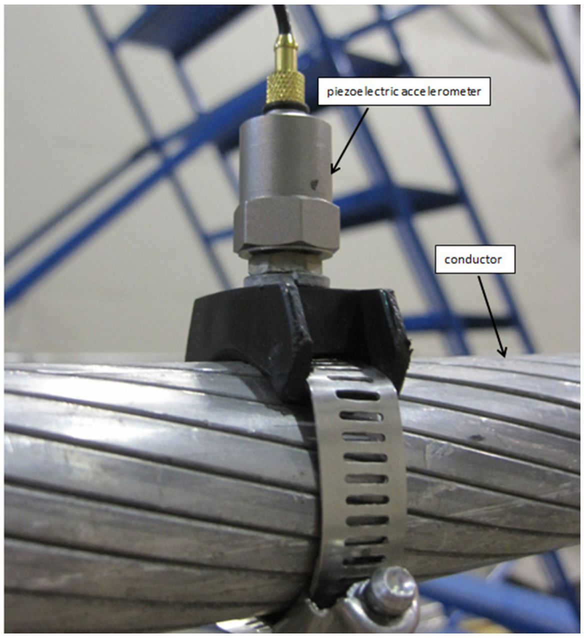

Fig. 7 Free loop accelerometer

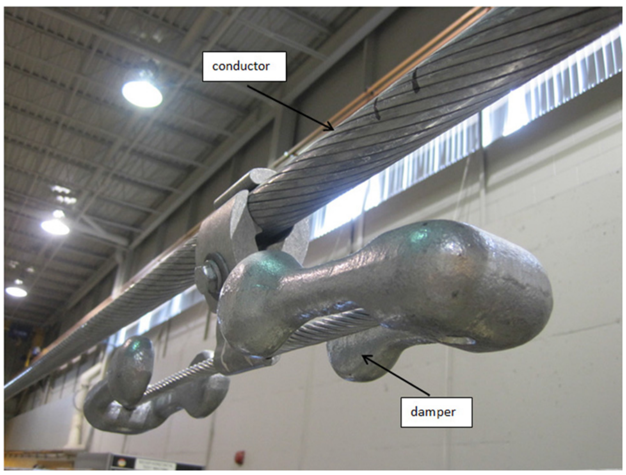

Fig. 8 Conductor with Stockbridge damper

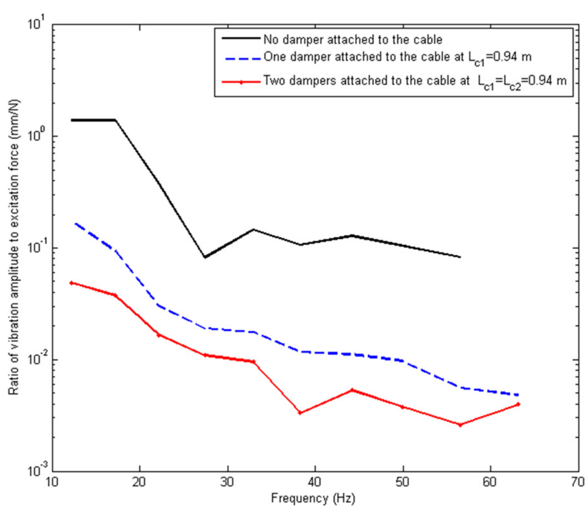

Fig. 9 Experiment results for damper effectiveness

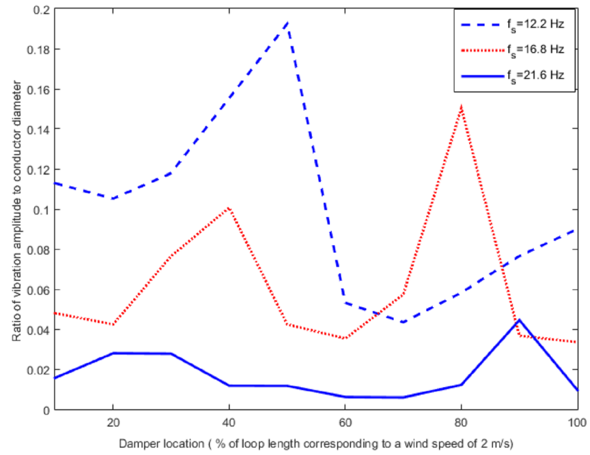

Fig. 10 Damper location optimization for lower frequencies

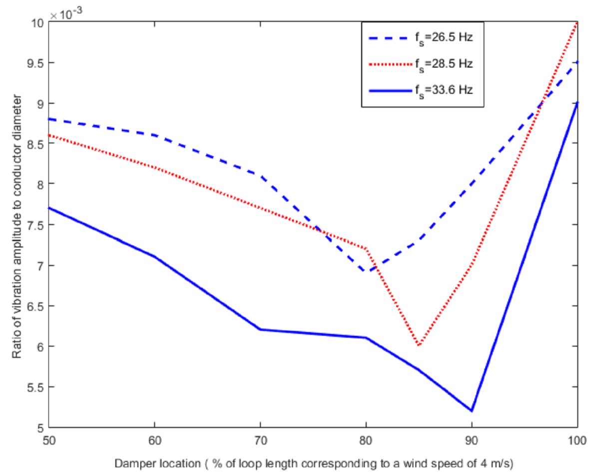

Fig. 11 Damper location optimization for medium frequencies

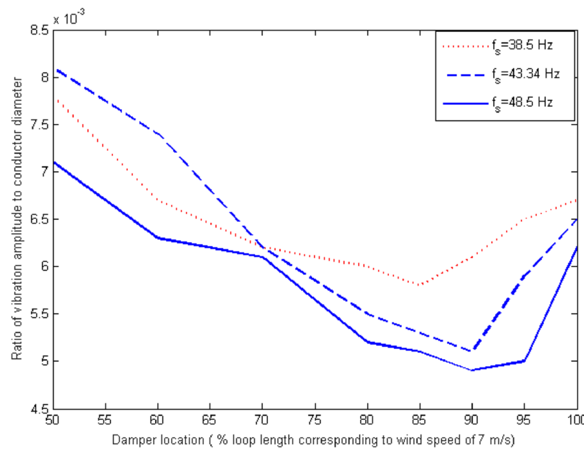

Fig. 12 Damper location optimization for higher frequencies

Fig. 13, and they indicate that positioning the bigger mass such that it points toward the tower slightly ameliorates the performance of the Stockbridge damper. The experimental results presented in Fig. 14 show similar trends as those in Fig. 13.

In the second part of the numerical analysis, a span length of $L_c = 366$ m is selected. This selection ensures that the conductor sag to span length ratio is typical of existing transmission lines (i.e., 0.03). The equivalent wind force $F_0 = 370.9$ N is used. The

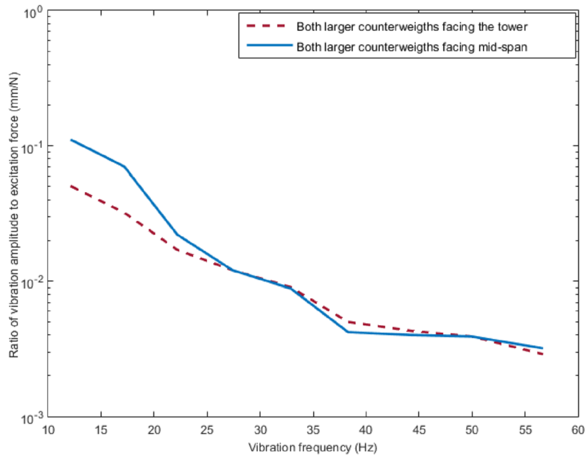

Fig. 13 Analytical results for orientation of the counterweight (one damper per span)

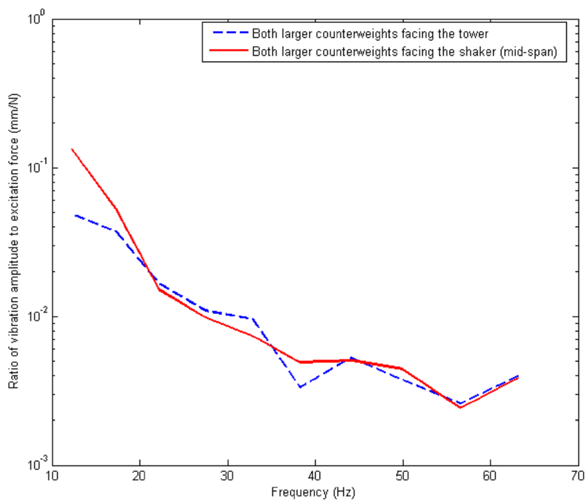

Fig. 14 Experiment results for orientation of the counterweight (two dampers per span)

bending strain ($\epsilon = \pi DYf\sqrt{(m/T)}$) is employed in the subsequent numerical examples because it is a measure of the severity of Aeolian vibration [11].

In Fig. 15, a comparison between the symmetric arrangement (proposed damping arrangement in Ref. [1]) and asymmetric damping arrangement is examined. These results clearly indicate that all the three scenarios of the asymmetric damping arrangement perform better than the symmetric damping arrangement. The symmetric arrangement shows very good control for high frequencies, but poor control for low frequencies. All the three asymmetric damping arrangement scenarios show very good control for both low and high excitation frequencies. Hence, the asymmetric damping arrangement is recommended for the control of Aeolian vibration of transmission lines.

An optimal damping arrangement would, therefore, involve one damper located between 50% and 70% of the loop length, corresponding to the lowest wind speed, and another damper located between 85% and 90% of the loop length, corresponding to the highest wind speed. The experimental results in Fig. 16 indicate that the performance of symmetrical damping arrangements is not very different from that of asymmetrical damping arrangements. This was due to the fact that the selected damper location values for the asymmetric damping arrangement were not the optimum.

To further investigate the validity of the proposed algorithm, the results obtained using the MATLAB built-in routine *fmincon* are

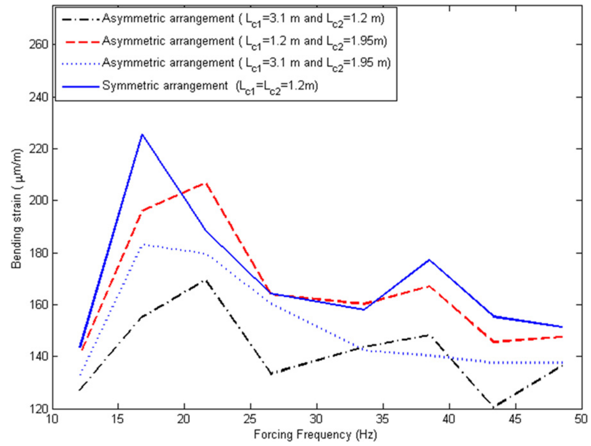

Fig. 15 Analytical results for symmetric versus asymmetric arrangement

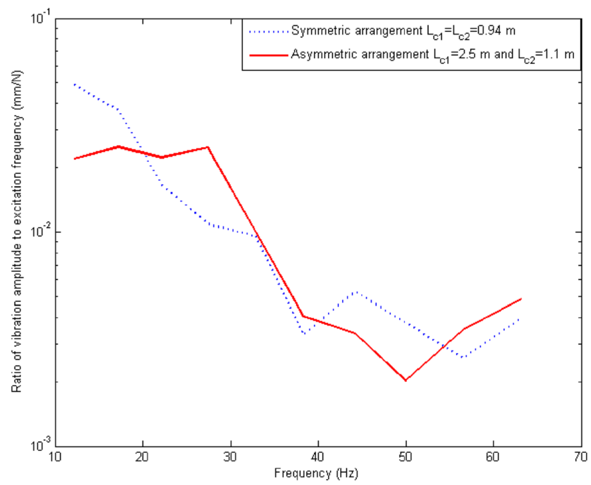

Fig. 16 Experimental results for symmetric versus asymmetric arrangement

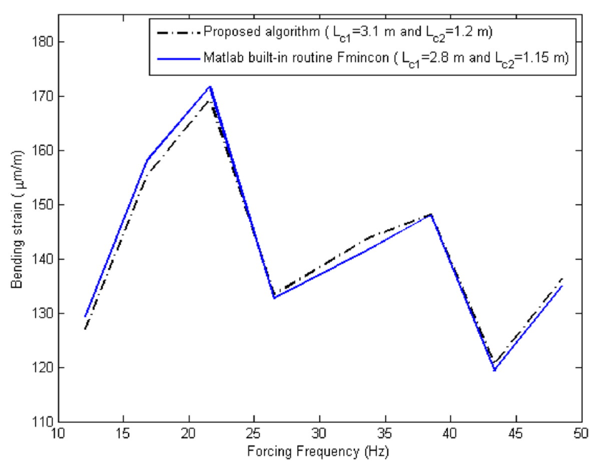

Fig. 17 Proposed heuristic algorithm versus MATLAB optimization using *fmincon* routine

compared with those obtained using the proposed algorithm. The optimal damper location for the proposed algorithm is taken to be 3.1 and 1.2 m from each end, and the results of the *fmincon* command indicate that the optimal damper location is 2.7 and 1.15 m from each end. It is noted that the results of the *fmincon* command correspond to 58.6% of the loop length, corresponding to 2 m/s, and 87.1% of the loop length, corresponding to 7 m/s, respectively. A further illustration of this corroboration is demonstrated in Fig. 17, where the difference between the two methods is observed to be negligible. Hence, the proposed rational approach is considered a worthy alternative method for determining the optimal damper location.

5 Conclusions

The state-of-the art of damper placement on transmissions lines for controlling vibrations is based on a rule of thumb. This rule of thumb is revisited in this paper by not only using the highest wind speed but also by including both low and medium wind speeds. An explicit expression of the loop length was presented. A rational approach was proposed to determine the optimal damper location, and the results were validated numerically using a MATLAB optimization routine and experimentally using the results obtained from experiments.

The experimental results comparing asymmetric and symmetric damping arrangement were inconclusive due to the fact that the values employed for the asymmetric location were not the optimum. The analytical results, however, demonstrated that the asymmetric damping arrangement performs better than the symmetric arrangement provided that the optimum location was correctly chosen. It was demonstrated that the optimal location of the damper involved placing one damper between 50% and 70% of the loop length corresponding to low wind speed (2 m/s) and another damper 85–95% of the loop length corresponding to high wind speed (7 m/s). It was also observed that the orientation of the bigger counterweight toward the tower slightly improves the effectiveness of the Stockbridge damper.

Acknowledgment

The financial assistance from Hydro One, Inc. is acknowledged. The authors are also grateful to Mr. Andrew Rizzetto of Kinectrics, Inc., Toronto, ON, Canada for his assistance with the experiments.

Appendix

For the sake of simplicity, the following notations are used:

$$\begin{aligned} s_i &= \sin\alpha L_{c_i}, & sh_i &= \sin h\beta L_{c_i} \\ c_i &= \cos\alpha L_{c_i}, & ch_i &= \cos h\beta L_{c_i} \\ s_{\Omega i} &= \sin\Omega_m L_{m_i}, & sh_{\Omega i} &= \sin h\Omega_m L_{m_i} \\ c_{\Omega i} &= \cos\Omega_m L_{m_i}, & ch_{\Omega i} &= \sin h\Omega_m L_{m_i} \end{aligned}$$

where

$$\alpha = \sqrt{(-S^2/2) + \sqrt{(S^4/4) + \Omega_c^4}}$$

and

$$\beta = \sqrt{(S^2/2) + \sqrt{(S^4/4) + \Omega_c^4}}$$

$\Omega_c = (\omega^2 m_c/E_c I_c)^{\frac{1}{4}}$, $\Omega_m = (\omega^2 m_m/E_m I_m)^{\frac{1}{4}}$, and $S = \sqrt{T/E_c I_c}$.

By ignoring the hyperbolic function terms because the tension and the span length in transmission lines are usually very large, the conductor mode shapes for each segment can be expressed as [8]

$$Y_{c_1}(x) = \sin\alpha x_1 \tag{A1}$$

$$Y_{c_2}(x) = \frac{s_1}{s_2}\sin\alpha x_2 \tag{A2}$$

The mode shapes of the messenger are expressed as

$$\begin{aligned} Y_{mi}(x_m) &= B_{1i}\sin\Omega_m x_m + B_{2i}\cos\Omega_m x_m + B_{3i}\sin h\Omega_m x_m \\ &\quad + B_{4i}\cos h\Omega_m x_m - \left(Y^*_{c_1} + (-1)^{(i+1)} x_m Y'^*_{c_1}\right) \end{aligned} \tag{A3}$$

where the constants of integration are given as

$$\begin{aligned} B_{1i} = \frac{1}{\lambda_i}\{&\mathcal{F}_{11,1}\mathcal{F}_{(i+4),7}\mathcal{F}_{(i+6),8} - \mathcal{F}_{11,1}\mathcal{F}_{(i+4),7}\mathcal{F}_{(i+6),6} \\ &+ \mathcal{F}_{1,1}\mathcal{F}_{(i+4),6}\mathcal{F}_{(i+6),8} - \mathcal{F}_{1,1}\mathcal{F}_{(i+4),8}\mathcal{F}_{(i+6),6} \\ &- \mathcal{F}_{11,1}\mathcal{F}_{(i+4),8}\mathcal{F}_{(i+6),7} + \mathcal{F}_{11,1}\mathcal{F}_{(i+4),6}\mathcal{F}_{(i+6),7}\} \end{aligned} \tag{A4}$$

$$\begin{aligned} B_{2i} = -\frac{1}{\lambda_i}\{&-\mathcal{F}_{1,1}\mathcal{F}_{(i+6),8}\mathcal{F}_{(i+4),7} + \mathcal{F}_{1,1}\mathcal{F}_{(i+6),8}\mathcal{F}_{(i+4),5} \\ &+ \mathcal{F}_{1,1}\mathcal{F}_{(i+6),7}\mathcal{F}_{(i+4),8} - \mathcal{F}_{1,1}\mathcal{F}_{(i+6),5}\mathcal{F}_{(i+4),8} \\ &- \mathcal{F}_{11,1}\mathcal{F}_{(i+6),5}\mathcal{F}_{(i+4),7} + \mathcal{F}_{11,1}\mathcal{F}_{(i+6),7}\mathcal{F}_{(i+4),5}\} \end{aligned} \tag{A5}$$

$$\begin{aligned} B_{3i} = -\frac{1}{\lambda_i}\{&\mathcal{F}_{11,1}\mathcal{F}_{(i+6),8}\mathcal{F}_{(i+4),5} - \mathcal{F}_{11,1}\mathcal{F}_{(i+6),6}\mathcal{F}_{(i+4),5} \\ &+ \mathcal{F}_{1,1}\mathcal{F}_{(i+4),6}\mathcal{F}_{(i+6),8} - \mathcal{F}_{1,1}\mathcal{F}_{(i+4),8}\mathcal{F}_{(i+6),6} \\ &- \mathcal{F}_{11,1}\mathcal{F}_{(i+6),5}\mathcal{F}_{(i+4),8} + \mathcal{F}_{11,1}\mathcal{F}_{(i+6),5}\mathcal{F}_{(i+4),6}\} \end{aligned} \tag{A6}$$

$$\begin{aligned} B_{4i} = \frac{1}{\lambda_i}\{&-\mathcal{F}_{11,1}\mathcal{F}_{(i+6),5}\mathcal{F}_{(i+4),7} - \mathcal{F}_{1,1}\mathcal{F}_{(i+6),6}\mathcal{F}_{(i+4),7} \\ &+ \mathcal{F}_{1,1}\mathcal{F}_{(i+6),6}\mathcal{F}_{(i+4),5} + \mathcal{F}_{11,1}\mathcal{F}_{(i+6),7}\mathcal{F}_{(i+4),5} \\ &+ \mathcal{F}_{1,1}\mathcal{F}_{(i+6),7}\mathcal{F}_{(i+4),6} - \mathcal{F}_{1,1}\mathcal{F}_{(i+6),5}\mathcal{F}_{(i+4),6}\} \end{aligned} \tag{A7}$$

where

$$\begin{aligned} \lambda_i = \mathcal{F}_{(i+6),8}\mathcal{F}_{(i+4),7} &- \mathcal{F}_{(i+6),8}\mathcal{F}_{(i+4),5} - \mathcal{F}_{(i+6),6}\mathcal{F}_{(i+4),7} \\ &+ \mathcal{F}_{(i+6),8}\mathcal{F}_{(i+4),5} - \mathcal{F}_{(i+6),7}\mathcal{F}_{(i+4),8} + \mathcal{F}_{(i+6),7}\mathcal{F}_{(i+4),6} \\ &+ \mathcal{F}_{(i+6),5}\mathcal{F}_{(i+4),8} - \mathcal{F}_{(i+6),5}\mathcal{F}_{(i+4),6} \end{aligned}$$

and

$$\begin{aligned} F_{1,1} = s_1,\quad F_{1,2} = sh_1,\quad F_{1,3} = -s_2,\quad F_{1,1} = -sh_2 \\ F_{2,1} = \alpha c_1,\ F_{2,2} = \beta ch_1,\ F_{2,3} = \alpha c_2,\ F_{2,4} = \beta ch_2 \end{aligned}$$

$$\mathcal{F}_{3,1} = \alpha c_1 h^2(m_1 + m_2 + m_{m_1} + m_{m_2}) + \frac{\alpha^2}{\omega^2}E_c I_c s_1$$

$$\mathcal{F}_{3,2} = \beta ch_1 h^2(m_1 + m_2 + m_{m_1} + m_{m_2}) - \frac{\beta^2}{\omega^2}E_c I_c sh_1$$

$$\mathcal{F}_{3,3} = -\frac{\alpha^2}{\omega^2}s_2 E_c I_c, \qquad \mathcal{F}_{3,4} = \frac{\beta^2}{\omega^2}sh_2 E_c I_c$$

$$\mathcal{F}_{3,5} = m_1 L_{m_1} s_{\Omega 1} + \Omega_m c_{\Omega 1} I_1 + m_m\left(-\frac{L_{m_1} c_{\Omega 1}}{\Omega_m} + \frac{1}{\Omega_m^2}s_{\Omega 1}\right)$$

$$\mathcal{F}_{3,6} = m_1 L_{m_1} c_{\Omega 1} - \Omega_m s_{\Omega 1} I_1 + m_m\left(\frac{L_{m_1} s_{\Omega 1}}{\Omega_m} + \frac{1}{\Omega_m^2}(c_{\Omega 1} - 1)\right)$$

$$\mathcal{F}_{3,7} = m_1 L_{m_1} sh_{\Omega 1} + \Omega_m ch_{\Omega 1} I_1 + m_m\left(\frac{L_{m_1} ch_{\Omega 1}}{\Omega_m} - \frac{1}{\Omega_m^2}sh_{\Omega 1}\right)$$

$$\mathcal{F}_{3,8} = m_1 L_{m_1} ch_{\Omega 1} + \Omega_m sh_{\Omega 1} I_1 + m_m\left(\frac{L_{m_1} sh_{\Omega 1}}{\Omega_m} - \frac{1}{\Omega_m^2}(ch_{\Omega 1} - 1)\right)$$

$$\mathcal{F}_{3,9} = -m_2 L_{m_2} s_{\Omega 2} - \Omega_{\rm m} c_{\Omega 2} I_2 - m_{\rm m}\left(-\frac{L_{m_2} c_{\Omega 2}}{\Omega_{\rm m}} + \frac{1}{\Omega_{\rm m}^2} s_{\Omega 2}\right)$$

$$\mathcal{F}_{3,10} = -m_2 L_{m_2} c_{\Omega 2} + \Omega_{\rm m} s_{\Omega 2} I_2 - m_{\rm m}\left(\frac{L_{m_2} s_{\Omega 2}}{\Omega_{\rm m}} + \frac{1}{\Omega_{\rm m}^2}(c_{\Omega 2} - 1)\right)$$

$$\mathcal{F}_{3,11} = -m_2 L_{m_2} sh_{\Omega 2} - \Omega_{\rm m} ch_{\Omega 2} I_2 - m_{\rm m}\left(\frac{L_{m_2} ch_{\Omega 2}}{\Omega_{\rm m}} - \frac{1}{\Omega_{\rm m}^2} sh_{\Omega 2}\right)$$

$$\begin{aligned}\mathcal{F}_{3,12} = &-m_2 L_{m_2} ch_{\Omega 2} - \Omega_{\rm m} sh_{\Omega 2} I_2 \\ &- m_{\rm m}\left(\frac{L_{m_2} sh_{\Omega 2}}{\Omega_{\rm m}} - \frac{1}{\Omega_{\rm m}^2}(ch_{\Omega 2} - 1)\right)\end{aligned}$$

$$\mathcal{F}_{4,1} = \frac{-\alpha^3}{\omega^2} c_1 E_{\rm c} I_{\rm c}, \qquad \mathcal{F}_{4,2} = \frac{\beta^3}{\omega^2} ch_1 E_{\rm c} I_{\rm c}$$

$$\mathcal{F}_{4,3} = \frac{-\alpha^3}{\omega^2} c_2 E_{\rm c} I_{\rm c}, \qquad \mathcal{F}_{4,4} = \frac{\beta^3}{\omega^2} ch_2 E_{\rm c} I_{\rm c}$$

$$\mathcal{F}_{4,5} = m_1 s_{\Omega 1} - \frac{m_{\rm m}}{\Omega_{\rm m}}(c_{\Omega 1} - 1), \qquad \mathcal{F}_{4,6} = m_1 c_{\Omega 1} + \frac{m_{\rm m}}{\Omega_{\rm m}} s_{\Omega 1}$$

$$F_{4,7} = m_1 sh_{\Omega 1} + \frac{m_{\rm m}}{\Omega_{\rm m}}(ch_{\Omega 1} - 1), \quad F_{4,8} = m_1 ch_{\Omega 1} + \frac{m_{\rm m}}{\Omega_{\rm m}} sh_{\Omega 1}$$

$$\mathcal{F}_{4,9} = m_2 s_{\Omega 2} - \frac{m_{\rm m}}{\Omega_{\rm m}}(c_{\Omega 2} - 1), \qquad \mathcal{F}_{4,10} = m_2 c_{\Omega 2} + \frac{m_{\rm m}}{\Omega_{\rm m}} s_{\Omega 2}$$

$$F_{4,11} = m_2 sh_{\Omega 2} + \frac{m_{\rm m}}{\Omega_{\rm m}}(ch_{\Omega 2} - 1), \quad F_{4,12} = m_2 ch_{\Omega 2} + \frac{m_{\rm m}}{\Omega_{\rm m}} sh_{\Omega 2}$$

$$F_{5,5} = s_{\Omega 1} - \lambda_{m_1}\Omega_{\rm m}^3 c_{\Omega 1}, \qquad F_{5,6} = c_{\Omega 1} + \lambda_{m_1}\Omega_{\rm m}^3 s_{\Omega 1}$$

$$\mathcal{F}_{5,7} = sh_{\Omega 1} + \lambda_{m_1}\Omega_{\rm m}^3 ch_{\Omega 1}, \quad \mathcal{F}_{5,8} = ch_{\Omega 1} + \lambda_{m_1}\Omega_{\rm m}^3 sh_{\Omega 1}$$

$$\mathcal{F}_{6,9} = s_{\Omega 2} - \lambda_{m_2}\Omega_{\rm m}^3 c_{\Omega 2}, \qquad \mathcal{F}_{6,10} = c_{\Omega 2} + \lambda_{m_2}\Omega_{\rm m}^3 s_{\Omega 2}$$

$$\mathcal{F}_{6,11} = sh_{\Omega 2} + \lambda_{m_2}\Omega_{\rm m}^3 ch_{\Omega 2}, \quad \mathcal{F}_{6,12} = ch_{\Omega 2} + \lambda_{m_2}\Omega_{\rm m}^3 sh_{\Omega 2}$$

$$\mathcal{F}_{7,5} = c_{\Omega 1} + \kappa_{m_1}\Omega_{\rm m} s_{\Omega 1}, \quad \mathcal{F}_{7,6} = -s_{\Omega 1} + \kappa_{m_1}\Omega_{\rm m} c_{\Omega 1}$$

$$F_{7,7} = ch_{\Omega 1} - \kappa_{m_1}\Omega_{\rm m} sh_{\Omega 1}, \quad F_{7,8} = sh_{\Omega 1} - \kappa_{m_1}\Omega_{\rm m} ch_{\Omega 1}$$

$$F_{8,9} = c_{\Omega 2} + \kappa_{m_2}\Omega_{\rm m} s_{\Omega 2}, \quad F_{8,10} = -s_{\Omega 2} + \kappa_{m_2}\Omega_{\rm m} c_{\Omega 2}$$

$$\mathcal{F}_{8,11} = ch_{\Omega 2} - \kappa_{m_2}\Omega_{\rm m} sh_{\Omega 2}, \quad \mathcal{F}_{8,12} = sh_{\Omega 2} - \kappa_{m_2}\Omega_{\rm m} ch_{\Omega 2}$$

$$\mathcal{F}_{9,1} = \mathcal{F}_{10,1} = -s_1, \qquad \mathcal{F}_{9,2} = \mathcal{F}_{10,2} = -sh_1$$

$$\mathcal{F}_{9,6} = \mathcal{F}_{9,8} = \mathcal{F}_{10,10} = \mathcal{F}_{10,12} = 1$$

$$\mathcal{F}_{11,1} = \frac{-\alpha c_1}{\Omega_{\rm m}}, \qquad \mathcal{F}_{11,2} = \frac{-\beta ch_1}{\Omega_{\rm m}}$$

$$F_{12,1} = -F_{11,1}, \qquad F_{12,2} = -F_{11,2}$$

References

[1] EPRI, 2006, "EPRI Transmission Line Reference Book, Wind Induced Conductor Motion," Electrical Power Research Institute, Palo Alto, CA.

[2] Lu, M. L., and Chan, J. K., 2007, "An Efficient Algorithm for Aeolian Vibration of Single Conductor With Multiple Dampers," IEEE Trans. Power Delivery, **22**(3), pp. 1822–1829.

[3] Nigol, O., and Houston, H. J., 1985, "Aeolian Vibration of Single Conductor and Its Control," IEEE Trans. Power Delivery, **104**(11), pp. 3245–3254.

[4] Kraus, M., and Hagedorn, P., 1991, "Aeolian Vibration: Wind Energy Input Evaluated From Measurements on an Energized Transmission Lines," IEEE Trans. Power Delivery, **6**(3), pp. 1264–1270.

[5] Barry, O., Oguamanam, D. C. D., and Lin, D. C., 2013, "Aeolian Vibration of a Single Conductor With a Stockbridge Damper," Proc. Inst. Mech. Eng., Part C, **227**(5), pp. 935–945.

[6] Claren, R., and Diana, G., 1969, "Mathematical Analysis of Transmission Line Vibration," IEEE Trans. Power Delivery, **60**(2), pp. 1741–1771.

[7] Verma, H., and Hagerdorn, P., 2004, "Wind Induced Vibration of Long Electrical Overhead Transmission Line Spans: A Modified Approach," J. Wind Struct., **8**(2), pp. 89–106.

[8] Barry, O., Zu, J. W., and Oguamanam, D. C. D., 2013, "Analytical and Experimental Investigation of Overhead Transmission Line Vibration," J. Vib. Control, **21**(14), pp. 2825–2837.

[9] Barry, O., Zu, J. W., and Oguamanam, D. C. D., 2014, "Forced Vibration of Overhead Transmission Line: Analytical and Experimental Investigation," ASME J. Vib. Acoust., **136**(4), p. 041012.

[10] Barry, O., Zu, J. W., and Oguamanam, D. C. D., 2015, "Nonlinear Dynamics of Stockbridge Dampers," ASME J. Dyn. Syst. Meas. Control, **137**(6), p. 061017.

[11] Vecchiarelly, J., Curries, I. G., and Havard, D. G., 2000, "Computational Analysis of Aeolian Conductor Vibration With a Stockbridge-Type Damper," J. Fluid Struct., **14**(4), pp. 489–509.